



# Photoluminescence excitation spectroscopy of excited states of an asymmetric cubic GaN/Al<sub>0.25</sub>Ga<sub>0.75</sub>N double quantum well grown by molecular beam epitaxy

Tobias Wecker<sup>1\*</sup>, Gordon Callsen<sup>2</sup>, Axel Hoffmann<sup>2</sup>, Dirk Reuter<sup>1</sup>, and Donat J. As<sup>1\*</sup>

<sup>1</sup>Department of Physics, University of Paderborn, 33098 Paderborn, Germany

<sup>2</sup>Institut für Festkörperphysik, Technische Universität Berlin, 10623 Berlin, Germany

\*E-mail: wtobias@mail.uni-paderborn.de; d.as@uni-paderborn.de

Received November 18, 2015; revised December 8, 2015; accepted December 10, 2015; published online March 2, 2016

Optical transitions involving higher energy levels of cubic AlGa<sub>x</sub>N quantum wells are investigated by means of photoluminescence excitation spectroscopy. An asymmetric cubic GaN/Al<sub>x</sub>Ga<sub>1-x</sub>N double quantum well (QW) structure with an Al content of  $x = 0.25 \pm 0.03$  was grown on a 3C-SiC(001) substrate exploiting radio-frequency plasma-assisted molecular beam epitaxy. The photoluminescence excitation data reveals two emission bands, which are assigned to the first electron and the third heavy hole (e1–hh3) and the second electron and the second heavy hole (e2–hh2) energy level of the wide QW. Besides in the narrow QW no higher energy levels can be observed. The experimental data is in good agreement with theoretical calculations using a Schrödinger–Poisson solver based on an effective mass model (nextnano<sup>3</sup>). The exciton binding energy was calculated considering the confinement of the QWs and also the energy dependency of the effective mass for excited energy levels.  
© 2016 The Japan Society of Applied Physics

## 1. Introduction

The material system of the group III–nitrides has several advantages, for example the high endurance against mechanical, thermal, and chemical stress. Thus devices based on III–nitrides materials can be used for light emission and harvesting applications in harsh environments, as well as for high power electronics. Furthermore, the inherent large band offset between, e.g., GaN/AlN and their compounds enables large band gap variations, favorable for devices based on intraband transitions such as THz devices, fast modulators and fast photo detectors.<sup>1)</sup> As a result, the intersubband transitions in these GaN/AlN devices can cover the 1.55 μm spectral region (optical C-band),<sup>2)</sup> needed for telecommunication applications. Also Al<sub>x</sub>Ga<sub>1-x</sub>N as a compound material permits another degree of freedom and can be exploited for tailoring the bandgap in future heterostructure devices. Utilizing Al<sub>x</sub>Ga<sub>1-x</sub>N is especially suited for an efficient tuning of the required quantum well (QW) energy levels. For modern optoelectronic devices the knowledge and manipulation of the exact position of each energy level of electrons and holes is of high significance. Here, photoluminescence excitation (PLE) spectroscopy can serve as an ideal tool for investigating the precise energetic positioning of the electronic levels. Tuning the wavelength of the excitation source gives direct access to the related absorption but also to charge carrier transfer processes by monitoring the luminescence signal. Hence, not only the charge carrier transfer from, e.g., the barrier material into the QWs can be observed but even inter QW coupling processes (or their suppression) can experimentally be witnessed.<sup>3)</sup>

Common hexagonal group III–nitrides suffer from large internal polarization fields along the *c*-axis resulting in a bending of the bands and the quantum confined Stark-effect. Due to both effects the design of modern devices for intraband transitions in the hexagonal phase is reasonably complicated caused by the extended number of degrees of freedom involved.<sup>4)</sup> Besides, the efficiency of devices based on interband emission is reduced, because of the spatial separation of the electron and the hole wavefunction. In order to reduce these effects the growth of hexagonal nitrides in

semi-polar directions is intensively investigated.<sup>5)</sup> Another approach is the growth in the cubic phase in the (001) direction on 3C-SiC. Hence, all above listed unfavorable effects can significantly be suppressed along the growth axis.

In this work we study the energy levels in a cubic GaN/Al<sub>x</sub>Ga<sub>1-x</sub>N asymmetric double quantum well (ADQWs) by PLE measurements. Model calculations of the transition energies were performed with the Schrödinger–Poisson solver nextnano<sup>3</sup> (Ref. 6) yielding a good agreement.

## 2. Experimental methods

An asymmetric cubic GaN/Al<sub>x</sub>Ga<sub>1-x</sub>N double QW with an Al content of  $x = 0.25 \pm 0.03$  was grown on a 10 μm 3C-SiC (001) layer deposited on a 0.5-mm-thick Si substrate. The applied growth system comprises a Riber-32 radio-frequency plasma-assisted molecular beam epitaxy (PAMBE) equipped with standard effusion cells for Ga and Al evaporation. The nitrogen is delivered by an Oxford plasma source and the growth process is in situ controlled by reflection high energy electron diffraction (RHEED). The growth at a substrate temperature of  $T_S = 720$  °C under one monolayer of Ga excess on the surface provides the best sample qualities for cubic GaN (c-GaN) and c-Al<sub>x</sub>Ga<sub>1-x</sub>N. Deeper insight into the growth of cubic GaN on 3C-SiC can be obtained based on Ref. 7. Atomic force microscopy measurements revealed an rms surface roughness of around 2 nm for  $5 \times 5 \mu\text{m}^2$  areas.

A 130 nm thick c-GaN buffer layer was directly grown on the 3C-SiC substrate. Subsequently, the ADQW structure was deposited. The barrier thickness between a wide (3.15 nm thickness) quantum well (QW<sub>W</sub>) and a narrow (0.9 nm thickness) quantum well (QW<sub>N</sub>) amounts to 15 nm. Hence, both quantum wells can be considered to be uncoupled.<sup>8)</sup> Nevertheless this sample can be used as a starting point for further investigations with coupled QWs. The ADQW structure is situated in between two 50 nm thick cubic Al<sub>0.25</sub>Ga<sub>0.75</sub>N layers. The entire sample structure is depicted in Fig. 1.

The structural sample properties were obtained by high resolution X-ray diffraction (HRXRD) measurements yielding reciprocal space map (RSM). An average defect density of the order of  $D = 2 \times 10^{10} \text{ cm}^{-2}$  was obtained by measuring

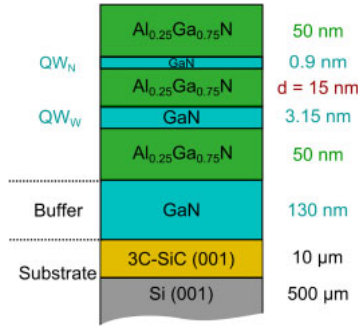


**Fig. 1.** (Color online) Sample structure of the cubic GaN/Al<sub>0.25</sub>Ga<sub>0.75</sub>N ADQW. The barrier thickness between the two QWs is 15 nm, thus the wells are uncoupled.

the rocking curve full width half maxima around the (002) reflection. From the RSM around the (113) reflection of the ADQW sample an Al content of  $x = 0.25 \pm 0.03$  was determined. The RSM measurements also revealed the degree of relaxation  $R$  of the layers. The Al<sub>0.25</sub>Ga<sub>0.75</sub>N layers are partly tensilely strained in regard to the GaN buffer layer, thus an equilibrium lattice parameter is established in the ADQW structure leading to partly compressively strained QWs.

### 3. Results and discussion

#### 3.1 Nextnano<sup>3</sup> simulations

Simulations of the band structure are performed in order to obtain a detailed understanding of the experimental data. A Schrödinger–Poisson solver (nextnano<sup>3</sup>, Ref. 6) was used to determine the energy levels of the structure as well as the allowed interband transitions. Calculations with nextnano<sup>3</sup> are based on an effective mass model. For the valence band conduction band offset between GaN and AlN the value 74 : 26<sup>9)</sup> was used. In all calculations a background n-type doping of around  $5 \times 10^{17} \text{ cm}^{-3}$  in Al<sub>x</sub>Ga<sub>1-x</sub>N and of around  $1 \times 10^{17} \text{ cm}^{-3}$  in GaN is assumed.<sup>10)</sup> Other necessary parameters for nextnano<sup>3</sup> are summarized in Table I. All the parameters have been linearly interpolated between GaN and AlN for AlGa<sub>x</sub>N. Only the bandgap  $E_{\text{gap}}$  was interpolated quadratically using the bowing parameter  $b = 0.85$ .<sup>11)</sup>

The QW thickness commonly differs by  $\pm 1$ –2 monolayers [one monolayer (1 ML) of c-GaN is 0.225 nm] due to growth restrictions. The best match of simulated energy levels and the PLE measurements (Figs. 4 and 5) is achieved for a 0.9 and 3.375 nm QW at 7 K. In the nextnano<sup>3</sup> calculations no excitonic effects are considered. They are calculated independently analog to Ref. 20 and are subsequently taken into account. Due to the different masses of light holes (lh) and heavy holes (hh) the calculated excitonic binding energies are also different if the exciton (X) is formed by an electron (e) and hh ( $X_{e\text{-hh}}$ ) or e and lh ( $X_{e\text{-lh}}$ ). Furthermore the exciton binding energy changes for excited energy levels, due to the energy dependency of the effective mass  $m^*(\epsilon)$ . This is also considered using a modified Kane formula:<sup>9,21,22)</sup>

$$\frac{m_0}{m^*(\epsilon)} = 1 + 2F + \frac{E_p}{3} \left( \frac{2}{E_g + \epsilon} + \frac{1}{E_g + \Delta_{\text{so}} + \epsilon} \right). \quad (1)$$

With the confinement energy  $\epsilon$ , the interband matrix element for c-GaN  $E_p = 16.86 \text{ eV}$ ,<sup>9,23)</sup> a coupling constant of remote bands  $F$ , and the spin–orbit splitting of the valence band  $\Delta_{\text{so}} = 15 \text{ meV}$  (see Table I). The value for  $F$  is estimated in

**Table I.** Collection of the most important parameters of c-GaN and c-AlN used for nextnano<sup>3</sup>.

Parameter	c-GaN	c-AlN
$E_{\text{gap},0\text{K}}$ (eV)	3.293 <sup>12)</sup>	5.997 <sup>13)</sup>
$E_{\text{gap},300\text{K}}$ (eV)	3.23 <sup>12)</sup>	5.93 <sup>14)</sup>
$E_{\text{exciton}}$ (meV)	24 <sup>12)</sup>	—
$a$ (Å)	4.503 <sup>15)</sup>	4.373 <sup>16)</sup>
$m_e^*/m_0$	0.19 <sup>17)</sup>	0.3 <sup>17)</sup>
$m_{\text{hh}}^*/m_0$	0.83 <sup>17)</sup>	1.32 <sup>17)</sup>
$m_{\text{lh}}^*/m_0$	0.28 <sup>17)</sup>	0.44 <sup>17)</sup>
$m_{\text{so}}^*/m_0$	0.34 <sup>17)</sup>	0.55 <sup>17)</sup>
$\Delta_{\text{so}}$ (meV)	15 <sup>12)</sup>	19 <sup>17)</sup>
$\epsilon_r$	9.44 <sup>12)</sup>	8.07 <sup>14)</sup>
$\epsilon_\infty$	5.31 <sup>12)</sup>	4.25 <sup>14)</sup>
$c_{11}$ (GPa)	293 <sup>18)</sup>	304 <sup>18)</sup>
$c_{12}$ (GPa)	159 <sup>18)</sup>	160 <sup>18)</sup>
$c_{44}$ (GPa)	155 <sup>18)</sup>	193 <sup>18)</sup>
$a_g$ (eV)	−8.0 <sup>19)</sup>	−9.1 <sup>19)</sup>
$a_c = a_g + a_v$ (eV)	−6.0	−6.8
$a_v$ (eV)	2.0 <sup>19)</sup>	2.3 <sup>19)</sup>
$b_{\text{uniax}}$ (eV)	−1.7 <sup>19)</sup>	−1.5 <sup>19)</sup>

**Table II.** Summary of the excitonic binding energies ( $E_b$ ) for the two QW thicknesses. Due to different effective masses of light hole (lh) and heavy hole (hh) the excitonic binding energy change if the electron (e) interacts with an hh ( $X_{e\text{-hh}}$ ) or lh ( $X_{e\text{-lh}}$ ). Furthermore the energy dependence of the effective mass is considered.

QW thickness (nm)	$E_b$ (meV)				
	$X_{e1\text{-hh}1}$	$X_{e2\text{-hh}2}$	$X_{e1\text{-hh}3}$	$X_{e1\text{-lh}1}$	$X_{e2\text{-lh}2}$
3.375	35	37	26	33	25
0.9	36			32	

**Table III.** Overview of the theoretic transition energies and the fit curve maxima in the PLE and PL spectra. The excitonic binding energies (see Table II) are included.

Transition	Theory (eV)	PLE (eV)	PL (eV)
	QW <sub>W</sub>		
e1–hh1	3.37		3.36
e1–hh3	3.50	3.50	
e2–hh2	3.62	3.63	
QW <sub>N</sub>			
e1–hh1	3.60		3.61
e1–lh1	3.61		3.61

order to reach the bulk value for zero confinement ( $\epsilon = 0$ ).  $F$  is different for electron ( $F_e = -0.48$ ), heavy hole ( $F_{\text{hh}} = -2.50$ ) and light hole ( $F_{\text{lh}} = -1.32$ ).

The calculated binding energies are summarized in Table II. Furthermore in Table III the theoretical transitions are compared with the experimental data. Subsequently, we obtain an excellent agreement between theory and experiment, which only deviate by less than 10 meV.

Nextnano<sup>3</sup> cannot consider partial strain, only pseudo-morphical strained or unstrained structures can be treated. Thus the lattice constant of the cubic GaN buffer layer is adapted to achieve a partial strain of the ADQW structure as observed by HRXRD RSM. The lattice constant is interpolated linearly between the relaxed cubic GaN and

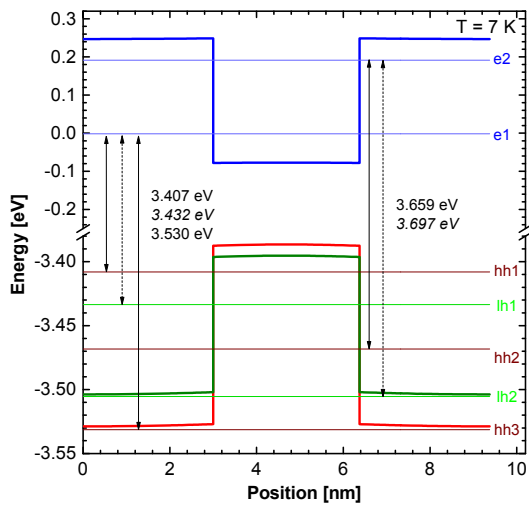


**Fig. 2.** (Color online) Simulation results of the energy levels and the band edges of the  $QW_W$  (3.375 nm) at a modeling temperature ( $T$ ) of 7 K. Two bound energy levels exist for the electrons (e), whereas the holes exhibit five bound states, three for the heavy holes (hh), and two for the light holes (lh). Therefore, five allowed transitions can occur.

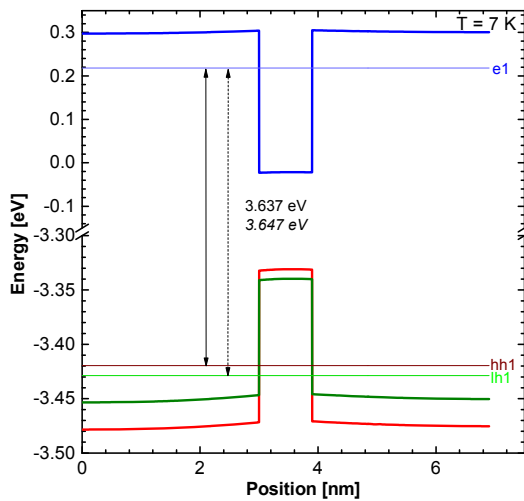


**Fig. 3.** (Color online) Simulation results of the energy levels and the band edges of the  $QW_N$  (0.9 nm) for a temperature ( $T$ ) of 7 K. There is one bound energy level in each time for the electrons (e), heavy holes (hh), and for the light holes (lh). Thus two allowed transitions are expected.

relaxed cubic  $Al_{0.25}Ga_{0.75}N$ . In that way the degree of relaxation of 0.4 for the  $Al_{0.25}Ga_{0.75}N$  barriers is achieved in the calculations, which was measured by HRXRD RSM along the (113) direction.<sup>8)</sup> In addition the degree of relaxation in the QWs is considered to be 0.6. In thick  $Al_xGa_{1-x}N$  bulk samples (>150 nm) a partial strain was measured even for  $x > 0.7$ , although the critical thickness is expected to be much lower. Thus we assume a constant partial strain level in our sample.

The ADQW is uncoupled, so the two QWs can be investigated independently. In Figs. 2 and 3 the conduction band edge (blue line) and the valence band edges are plotted vs the position along the growth direction for the  $QW_W$  (Fig. 2) and the  $QW_N$  (Fig. 3). Due to the residual strain in the QW structures, the band gaps for hh and lh deviate. Thus the transition energies for hh and lh energy levels differ regarding to the unstrained QW (red for hh, green for lh).

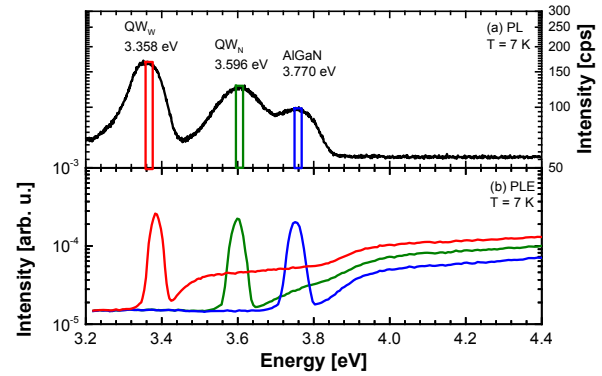


**Fig. 4.** (Color online) (a) Semi-logarithmic plot of the low temperature PL spectrum of the cubic  $GaN/Al_{0.25}Ga_{0.75}N$  ADQW at a temperature ( $T$ ) of 7 K. The depicted rectangles illustrate the applied detection for the PLE measurements. (b) Furthermore, PLE data for three different detection wavelengths with  $T = 7$  K are shown, which correspond to the emission maxima of the PL spectrum (red for the  $QW_W$ , green for the  $QW_N$ , blue for the  $Al_{0.25}Ga_{0.75}N$  barrier).

Furthermore, the bound energy levels for electrons, heavy holes, and light holes are plotted as dashed lines in Figs. 2 and 3 exhibiting a coloring that matches the corresponding band edges. Thus the simulation reveals the amount of bound energy levels for each carrier type. There are five allowed transitions for the  $QW_W$  and two for the  $QW_N$ .

To compare with the experiment for the e-hh and e-lh transitions also the excitonic binding energy has to be taken into account. Thus the hh3 and lh2 energy levels in Fig. 2 are bound, although the nextnano<sup>3</sup> levels are above the valence bands. Besides the excitonic binding energy is different for hh and lh excitons and for the different energy levels (see Table II). A detailed comparison with the PLE measurements shows a good agreement with the simulated transitions as described in the following.

### 3.2 PLE spectroscopy

Figure 4 depicts the low temperature interband PL measurements as well as the PLE measurements at a temperature of 7 K in a semi-logarithmic plot. A 500 W xenon short-arc lamp (XBO) was used for the optical excitation of the samples. In addition, for the PLE measurements the XBO lamp was guided through an additive double monochromator (SpectraPro) yielding a spectral resolution of about 3.2 nm. Three clearly distinguishable emission bands can be observed at 3.358, 3.596, and 3.770 eV and are associated to the  $QW_W$ , the  $QW_N$ , and the cubic  $Al_{0.25}Ga_{0.75}N$ , respectively. The transition energies of both QWs show a maximum difference of 10 meV with our nextnano<sup>3</sup> calculations (see Table III). Figure 4(b) depicted PLE spectra correspond to different detection wavelengths in agreement with the emission maxima of the different sample regions (red for the  $QW_W$ , green for the  $QW_N$ , blue for the  $Al_{0.25}Ga_{0.75}N$  barrier). Naturally, the PLE spectrum related to the emission maximum of the  $AlGaN$  barriers does only reveal the related band to band transition (blue curve). Also the green curve for the narrow QW show no additional features compared with ellipsometry data of bulk  $AlGaN$ .<sup>24)</sup> A pronounced step is visible in all PLE spectra at around 3.9 eV, which is a common feature of the band to band transition in bulk  $AlGaN$  as also observed<sup>24)</sup> by means of absorption measurements at

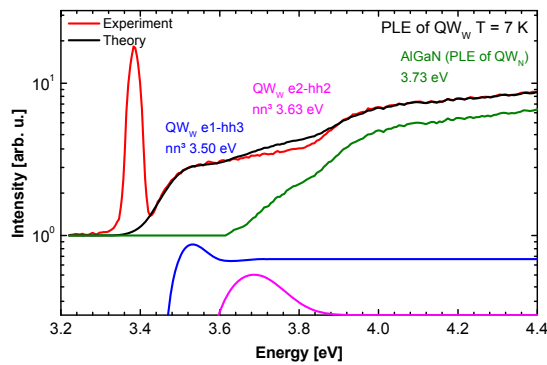


**Fig. 5.** (Color online) Detailed, semi-logarithmic plot of the low temperature PLE spectrum detected at the emission maximum of the  $QW_W$  at a temperature ( $T$ ) of 7 K. The narrow peak at 3.38 eV originates from an overlay of the excitation light and resonant sample luminescence. Furthermore, two transitions can be verified (e1–hh3 and e2–hh2) by a careful fitting routine.

room temperature. In contrast, the PLE spectrum of the  $QW_W$  shows additional spectral features at lower excitation energies as analyzed in the following. One interesting feature in all three PLE spectra is the high intensity of the sample luminescence compared to the excitation source.

Figure 5 depicts the PLE spectrum detected at the maximum emission of the  $QW_W$ . The simulations predict 5 allowed transitions, but only two can be identified. The low energy transition occurs between the first electron level (e1) and the third heavy hole level (hh3) at 3.50 eV. The high energy counterpart can be assigned to the second electron level (e2) and the second heavy hole (hh2) transition. Due to interface roughness effects this transition at 3.63 eV is broadened. As an approximation the intensity is fitted exploiting two gaussian functions with an error function to take into account the step behavior of the two-dimensional (2D) density of states. Besides the green curve used as background for the fit is the PLE spectra of the  $QW_N$ , which is caused by the AlGaIn barriers. The transitions below 3.4 eV could not be measured because of the high intensity of the source overlaid with the ground state emission visible as a narrow peak at 3.38 eV. The two QWs are uncoupled therefore the transitions cannot be assigned to the transition of the  $QW_N$ , although the energy is similar with 3.64 eV. The step at around 3.9 eV is a characteristic of band to band transitions in AlGaIn.<sup>24)</sup>

#### 4. Conclusions

An uncoupled asymmetric cubic GaN/Al<sub>0.25</sub>Ga<sub>0.75</sub>N double QW was grown by plasma assisted molecular beam epitaxy. High resolution X-ray diffractometry measurements provide the Al content of  $x = 0.25 \pm 0.03$ . A partial strain of the Al<sub>0.25</sub>Ga<sub>0.75</sub>N barriers is observed in the RSMs around the (113) reflection, leading to an equilibrium lattice parameter with tensilely strained Al<sub>x</sub>Ga<sub>1-x</sub>N barriers and compressively strained QWs. Photoluminescence measurements at 7 K show three different emission maxima corresponding to the two QWs and the AlGaIn barriers. A Schrödinger–Poisson solver based on an effective mass model (nextnano<sup>3</sup>) was used to simulate the corresponding band structure and the energy levels in order to enable a direct comparison to PLE measurements. In addition to the nextnano<sup>3</sup> simulations the

exciton binding energy was calculated considering the confinement of the QWs and also the energy dependency of the effective mass for excited energy levels. The PLE spectrum that are assigned to the wide QW emission reveals two transitions (e1–hh3, e2–hh2) and an additional step in the excitation characteristics, which belongs to the band to band transition of the AlGaIn barriers. The other PLE data belonging to the  $QW_N$  and the AlGaIn emission show no further transitions of excited states from the QW levels as confirmed by the nextnano<sup>3</sup> simulations. A very good prediction of the energy levels and transitions for the  $QW_W$  is found with a maximum deviation of 10 meV between theory and experiment.

#### Acknowledgments

This work has been financially supported by the Deutsche Forschungsgemeinschaft (DFG) via TRR142, by the Center for Optoelectronics and Photonics Paderborn (CeOPP), and by the Collaborative Research Center (CRC) 787.

- 1) H. Machhadani, M. Tchernycheva, L. Rigutti, S. Saki, R. Colombelli, C. Mietze, D. J. As, and F. H. Julien, *Phys. Rev. B* **83**, 075313 (2011).
- 2) C. Gmachl and H. M. Ng, *Electron. Lett.* **39**, 567 (2003).
- 3) M. Beeler, E. Trichas, and E. Monroy, *Semicond. Sci. Technol.* **28**, 074022 (2013).
- 4) M. Beeler, C. Bougerol, E. Bellet-Amalaric, and E. Monroy, *Phys. Status Solidi A* **211**, 761 (2014).
- 5) F. Scholz, *Semicond. Sci. Technol.* **27**, 024002 (2012).
- 6) S. Birner, S. Hackenbuchner, M. Sabathil, G. Zandler, J. A. Majewski, T. Andlauer, T. Zibold, R. Morschl, A. Trellakis, and P. Vogl, *Acta Phys. Pol. A* **110**, 111 (2006).
- 7) J. Schörmann, S. Potthast, D. J. As, and K. Lischka, *Appl. Phys. Lett.* **90**, 041918 (2007).
- 8) T. Wecker, F. Hörich, M. Feneberg, R. Goldhahn, D. Reuter, and D. J. As, *Phys. Status Solidi B* **252**, 873 (2015).
- 9) C. Mietze, M. Landmann, E. Rauls, H. Machhadani, S. Sakr, M. Tchernycheva, F. H. Julien, W. G. Schmidt, K. Lischka, and D. J. As, *Phys. Rev. B* **83**, 195301 (2011).
- 10) D. Bouguenna, A. Boudghene Stambouli, N. Mekkakia Maaza, A. Zado, and D. J. As, *Superlattices Microstruct.* **62**, 260 (2013).
- 11) M. Landmann, E. Rauls, W. G. Schmidt, M. Röppischer, C. Cobet, N. Esser, T. Schupp, D. J. As, M. Feneberg, and R. Goldhahn, *Phys. Rev. B* **87**, 195210 (2013).
- 12) M. Feneberg, M. Röppischer, C. Cobet, N. Esser, J. Schörmann, T. Schupp, D. J. As, F. Hörich, J. Bläsing, A. Krost, and R. Goldhahn, *Phys. Rev. B* **85**, 155207 (2012).
- 13) In h-AIN the difference in the energy gap from 0 to 300 K is about 67 meV.<sup>25,26)</sup> A similar value for c-AIN is assumed leading to  $E_{\text{gap},0\text{K}} = E_{\text{gap},300\text{K}} + 67 \text{ meV}$ .
- 14) M. Röppischer, R. Goldhahn, G. Rossbach, P. Schley, C. Cobet, N. Esser, T. Schupp, K. Lischka, and D. J. As, *J. Appl. Phys.* **106**, 076104 (2009).
- 15) T. Schupp, unpublished.
- 16) T. Schupp, K. Lischka, and D. J. As, *J. Cryst. Growth* **312**, 1500 (2010).
- 17) L. C. de Carvalho, A. Schleife, and F. Bechstedt, *Phys. Rev. B* **84**, 195105 (2011).
- 18) A. F. Wright, *J. Appl. Phys.* **82**, 2833 (1997).
- 19) C. G. Van de Walle and J. Neugebauer, *Appl. Phys. Lett.* **70**, 2577 (1997).
- 20) H. Mathieu, P. Lefebvre, and P. Christol, *Phys. Rev. B* **46**, 4092 (1992).
- 21) E. O. Kane, *J. Phys. Chem. Solids* **1**, 249 (1957).
- 22) C. Wetzel, R. Winkler, M. Drechsler, B. K. Meyer, U. Rössler, J. Scriba, J. P. Kotthaus, V. Härle, and F. Scholz, *Phys. Rev. B* **53**, 1038 (1996).
- 23) P. Rinke, M. Winkelnkemper, A. Qteish, D. Bimberg, J. Neugebauer, and M. Scheffler, *Phys. Rev. B* **77**, 075202 (2008).
- 24) M. Röppischer, Dissertation, Fakultät für Mathematik und Naturwissenschaften, TU Berlin, Berlin (2011).
- 25) M. Feneberg, M. F. Romero, M. Röppischer, C. Cobet, N. Esser, B. Neuschl, K. Thonke, M. Bickermann, and R. Goldhahn, *Phys. Rev. B* **87**, 235209 (2013).
- 26) I. Vurgaftman and J. R. Meyer, *J. Appl. Phys.* **94**, 3675 (2003).